Applied Catalysis B: Environmental 198 (2016) 420–430

Contents lists available at ScienceDirect

Applied Catalysis B: Environmental

journal homepage: www.elsevier.com/locate/apcatb

Simultaneous removal of elemental mercury and NO in simulated flue gas over V_2O_5/ZrO_2-CeO_2 catalyst

Lingkui Zhao[a,b], Caiting Li[a,b,*], Shanhong Li[a,b], Yan Wang[a,b], Junyi Zhang[a,b], Teng Wang[a,b], Guangming Zeng[a,b]

[a] College of Environmental Science and Engineering, Hunan University, Changsha 410082, PR China
[b] Key Laboratory of Environmental Biology and Pollution Control (Hunan University), Ministry of Education, Changsha 410082, PR China

ARTICLE INFO

Article history:
Received 26 January 2016
Received in revised form 21 May 2016
Accepted 30 May 2016
Available online 6 June 2016

Keywords:
V_2O_5
Elemental mercury
NH_3-SCR
CeO_2-ZrO_2
Nitrogen oxide

ABSTRACT

A series of V/$ZrCe_x$ catalyst synthesized by a co-precipitation method was employed to investigate the simultaneous removal of NO and elemental mercury (Hg^0) in simulated flue gas. The catalysts were characterized using BET, SEM, XRD, H_2–TPR, XPS, and FT–IR. V/$ZrCe_{0.6}$ with CeO_2/ZrO_2 molar ratio of 0.6 showed excellent SCR activity (87.3%) and high Hg^0 oxidation efficiency (77.6%) in SCR atmosphere (NH_3/NO = 1). The results indicated that the Hg^0 had little impact on NO conversion, while the coexistence of NO and O_2 would be beneficial for the Hg^0 oxidation. Hg^0 oxidation was inhibited in SCR atmosphere owing to the presence of NH_3. The characterization results demonstrated that the superior performance of V/$ZrCe_{0.6}$ catalyst might be attributed to lower crystallinity, better texture properties, strong redox ability and high reactive nitrate together with NH_3 species. The redox equilibrium ($Ce^{3+} + V^{5+} \leftrightarrow Ce^{4+} + V^{4+}$) contributed to the NO conversion and Hg^0 oxidation. The bidentate sulfates formed by adsorbed SO_2 could provide new acid sites for NH_3 adsorption and increase the amount of NH_4^+, which reduced the poisoning effect of SO_2 and H_2O. Based on the experimental results, a mechanism for the simultaneous removal of NO and Hg^0 was proposed for the V/$ZrCe_{0.6}$ catalysts: $2NH_3/NH_4^+(ad) + NO_2(ad) + NO(g) \rightarrow 2N_2 + 3H_2O + /2H^+$, $Hg(ad) + O\beta \rightarrow HgO(ad)$.

1. Introduction

Coal combustion is a major anthropogenic emissions source of NO_x and elemental mercury (Hg^0), which are considered as significant atmospheric contaminants and have attracted broad attention in recent years [1–3]. NO_x could lead to worsening local air quality, regional acid rain pollution and photochemical smog [4,5]. Mercury can be a threat to both human health and the environment due to the extreme toxicity, persistence, and the bioaccumulation [6,7]. Consequently, various environmental laws and regulations for the prevention and control of NO_x and Hg^0 pollutions have been enacted [8,9].

By far, the most successful and mature processes for controlling NO_x and Hg^0 are selective catalytic reduction (SCR) [10,11] and activated carbon injection (ACI) systems [12,13], respectively. However, the separate NO_x and Hg^0 control technology results in the low efficiency of apparatus, large equipment investment, and high operation cost [5]. As a result, the cost-effective methods that can remove NO_x and Hg^0 simultaneously need to be investigated. Recent studies indicated that catalysts employed in the selective catalytic reduction (SCR) of nitrogen oxides can promote the oxidation of Hg^0 [14–16]. Hence, SCR catalysts are one of the promising materials for simultaneous removal of NO and Hg^0, in which the key is to reduce NO by NH_3 and oxidize Hg^0 to the soluble Hg^{2+}. Although some metal oxides catalysts, such as Mn-Ce/Ti-PILCs, CeO_2–MoO_3, CeO_2–MnO_x/TiO_2, and V_2O_5–CeO_2/TiO_2, have been investigated for simultaneous removal of NO and Hg^0 [1,17–19], a systematic investigation on the influence mechanism of SO_2 as well as a connection between Hg^0 oxidation and NO conversion have rarely been reported.

Over the past few years, supported vanadium catalysts have attracted considerable attention due to their excellent advantages including high activity, selectivity and resistance to sulfur dioxide. In general, the nature of support was found to play a huge influence on the physicochemical and catalytic properties of the supported vanadium oxide catalysts [20]. Accordingly, scholars have tried a variety of vanadium based catalyst with different supports, such as alumina, zirconia and titania. As a typically support of SCR catalysts,

* Corresponding author at: College of Environmental Science and Engineering, Hunan University, Changsha 410082, PR China.
E-mail addresses: ctli@hnu.edu.cn, ctli3@yahoo.com (C. Li).

http://dx.doi.org/10.1016/j.apcatb.2016.05.079
0926-3373/

TiO_2 may not be ideal owing to its low specific surface area and poor thermal stability [21]. Due to unique physiochemical properties, ZrO_2 is widely used for catalysts, particularly employed as catalyst carrier in the SCR of NO_x by NH_3 [22]. CeO_2, can be utilized as catalyst support, promoter or even active species, possesses considerable oxygen storage capacity owing to the redox cycling between Ce^{3+} and Ce^{4+}, which has been already widely used as a crucial component in three-way catalysts (TWCs) [23]. In addition, there is a synergetic interaction between V_2O_5 (V) and CeO_2 (Ce), which could result in the high SCR performance and enhance the activity of Hg^0 oxidation [16,24]. However, pure CeO_2 showed poor stability and was susceptible sintering at high temperatures [25]. The insertion of ZrO_2 (Zr) into CeO_2 can improve the thermo-stability, mobility of lattice oxygen and the density of oxygen vacancies, because part of Ce^{4+} in CeO_2 is replaced by Zr^{4+} to form the cubic fluorite structure of CeZr mixed oxides. Therefore, there is reason to believe that CeZr supports may have good performance in SCR catalytic systems. Recently, CeZr–based catalysts were studied for SCR of NO with NH_3 [22,25,26]. For example, the V_2O_5/CeO_2–ZrO_2 (V/CeZr) catalysts showed high activity and selectivity for reduction of NO with NH_3 [22]. However, V_2O_5/ZrO_2–CeO_2 (V/ZrCe) has seldom been reported for simultaneous removal of NO and Hg^0.

The aim of this study was to understand the catalytic mechanism for simultaneous removal of Hg^0 and NO over V_2O_5/ZrO_2–CeO_2 and to clarify the effect mechanism of SO_2 on the reaction. A connection between Hg^0 oxidation and NO conversion was also systematically investigated. The physicochemical properties of the catalysts were systematically examined using some characterization methods including scanning electron microscopy (SEM), X–ray diffraction (XRD), Brunauer–Emmett–Teller (BET), temperature-programmed reduction of H_2 (H_2–TPR), X–ray Photoelectron Spectroscopy (XPS), and Fourier transform infrared spectroscopy (FT–IR).

2. Experimental

2.1. Synthesis of catalyst

ZrO_2–CeO_2 binary oxide supports were synthesized using a co-precipitation method. A certain amount of $Ce(NO_3)_3{\cdot}6H_2O$ and $ZrO(NO_3)_2{\cdot}2H_2O$ were used as precursors and dissolved in deionized water; the solutions were subsequently heated at 80 °C and stirred 30 min. After the solution cooled to room temperature, an aqueous solution of ammonia was added drop-wisely with vigorous stirring until the pH rose to 10. The resulting precipitates were stirred for 3 h and aged for 1 h at room temperature; after being filtered, the solid product was dried at 80 °C overnight, and then it was calcined at 500 °C for 4 h in air. The obtained ZrO_2–CeO_2 supports are denoted as $ZrCe_x$, where x represents the molar ratio of CeO_2/ZrO_2 (x = 0.2, 0.4, 0.6, 0.8, 1.0). The support materials of CeO_2 (Ce) and ZrO_2 (Zr) were prepared with the same process.

A series of V/Ce, V/Zr and V/$ZrCe_x$ catalysts were prepared by impregnating the support powders of Ce, Zr and $ZrCe_x$ with ammonium metavanadate solution for 12 h, and the molar ratio of V/Ce, V/Zr and V/$ZrCe_x$ was all 0.03. Then the samples were dried at 105 °C overnight and calcined at 500 °C for 3 h. Finally, the samples were crushed and sieved to 100–120 mesh.

2.2. Characterization

The catalyst microstructure was analyzed were determined by scanning electron microscopy (SEM) (Hitachi S-4800, Hitachi Limited, Japan). The separated areas for each catalyst were magnified to 100,000×.

The Brunauer–Emmett–Teller (BET) surface area, pore volume and average pore diameter of catalysts were obtained from N_2 adsorption isotherm using a Micromeritics Tristar II 3020 analyzer (Micromeritics Instrument Crop, USA). The specific surface area was calculated the N_2 desorption plots of the catalysts.

The crystalline phases of the catalysts were determined by X–ray diffractometer (Rigaku rotaflex D/Max–C, Japan) in the scattering angles (2θ) rang of 10–80° with Cu–Kα radiation (l = 1.5406 A°).

X–ray Photoelectron Spectroscopy (XPS) data were obtained on a K–Alpha 1063 system (Thermo Fisher Scientific, UK) with an Al Ka X–ray source. The binding energy (BE) was calibrated by C 1s at 284.6 eV.

The Fourier Transform Infrared Spectroscopy (FT–IR) was recorded on a FTIR–8400 S IRprestige-21 (SHIMADZU, Japan) apparatus. The IR spectra were recorded with 20 scans at a spectral resolution of 2 cm^{-1}. Prior to each measurement, the samples were treated at 250 °C in pure N_2 for 30 min to remove any adsorbed species, and cooled to room temperature. The total gas flow was 500 mL/min. The adsorption of NH_3 was carried out at room temperature for 1 h using a gaseous feed of 700 ppm NH_3/N_2. Subsequently, the FT–IR experiments were conducted immediately. A similar procedure was applied to study the NO + O_2 (700 ppm NO, 6% O_2/N_2), SO_2 + O_2 (300 ppmSO_2, 6% O_2/N_2), and SO_2 + H_2O + O_2 (300 ppmSO_2, 8 vol.% H_2O, 6% O_2/N_2) co-adsorption by treating the samples, respectively.

Temperature-programmed reduction of H_2 (H_2–TPR) was performed on a AutoChem 2920 automated chemisorption analyzer (Micromeritics Instrument Crop, USA) with approximately 1 g catalyst to analyze the redox properties of the catalysts. In order to eliminate the adsorbed volatile impurity, the catalysts were pretreated in pure N_2 at 300 °C for 30 min and then cooled to room temperature, performed in a flow of H_2 (5 vol.%) in Ar (40 mL/min) from 50 to 750 °C with a heating rate of 10 °C/min.

The temperature programmed desorption of ammonia (NH_3-TPD) was carried out using TP-5080 automatic chemical adsorption instrument (Tianjin Xian Quan, China). Prior to the experiment, the 200 mg sample was pretreated at 500 °C with a gas flow of He (30 mL/min) for 30 min. Then the samples were cooled down to 100 °C and exposed to NH_3 until saturation was reached, followed by flushing with pure He at the same temperature to avoid physisorption of NH_3. Afterwards, the NH_3-saturated samples were heated up to 600 °C at a heating rate of 10 °C/min in He.

2.3. Catalytic performance test

A schematic diagram of the experimental setup is shown in Fig. 1. The catalytic activity measurement for the removal of NO and Hg^0 was carried out at atmospheric pressure in a fixed bed continuous flow quartz reactor with i.d. 10 mm 0.25 g catalyst was placed in the reactor. The composition of simulated flue gas (SFG) including 700 ppm NO, 700 ppm NH_3, 6% O_2, 300 ppm SO_2 (when used), and N_2 (as balance) were precisely controlled by mass flow controllers (MFC). SCR atmosphere was defined as 6% O_2, 700 ppm of NO, and 280–700 ppm of NH_3 balanced in N_2. 70.0 μg/m^3 Hg^0 was generated by a Hg^0 permeation tube (VICI Metronics, USA). In order to avoid Hg^0 and water vapor condensation, all teflon tubes that Hg^0 and water vapor passed through were wrapped with a temperature-controlled heating tape and heated up to 120 °C. 8 vol.% H_2O (when used) was exactly controlled by peristaltic pump and injected into the teflon tube. 100 mL/min pure N_2 took along the water vapor to mix with the SFG. The gas was introduced into the reactor with the inlet flow rate at 500 mL/min, corresponding to a gas hourly space velocity (GHSV) of 100,000 h^{-1}. The steady-state tests were conducted from 100 to 400 °C. The NO and Hg^0 concentrations at the inlet ($NO_{in}/Hg^0{}_{in}$) and outlet ($NO_{out}/Hg^0{}_{out}$) of the reactor were measured respectively by a flue gas analyzer (MGA5, Germany) and an online RA–915 M mercury analyzer (LUMEX Ltd, Russia). Before proceeding to the mercury analyzer, acid gases and

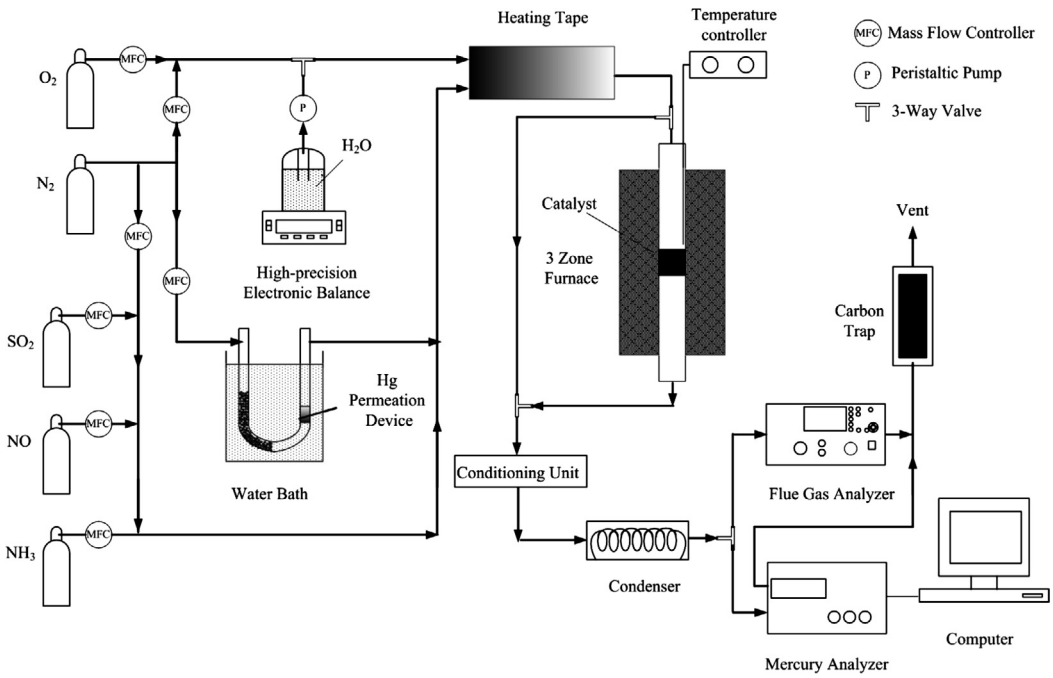

Fig. 1. Schematic diagram of the experimental setup.

NH_3 were removed by the conditioning unit which converged to a 10% NaOH solution. At the same time, water vapor was removed by the condenser. An adsorption experiment conducted at room temperature, and 0.25 g of V/ZrCe$_x$ catalysts were saturated with 70.0 μg/m^3 Hg^0 under N_2 atmosphere in less than 10 min, indicating that the Hg^0 physical adsorption capacity of the V/ZrCe$_x$ catalyst was negligible [27–29]. The decrease of Hg^0 concentration during an experiment was attributed to Hg^0 oxidation. Accordingly, the Hg^0 oxidation and NO conversion were respectively defined in Eqs. (1) and (2):

$$\eta_{Hg}(\%) = \frac{Hg^0_{in} - Hg^0_{out}}{Hg^0_{in}} \times 100\% \quad (1)$$

$$\eta_{NO}(\%) = \frac{NO_{in} - NO_{out}}{NO_{in}} \times 100\% \quad (2)$$

3. Results and discussion

3.1. Catalytic performance

3.1.1. Catalytic activity of V/ZrCe$_x$ catalysts

The simultaneous removal performances of NO and Hg^0 in SCR atmosphere (NH_3/NO = 1) were investigated at the temperature of 100–400 °C and the results are shown in Fig. 2. It was clear that the catalytic activity was influenced by the molar ratios of Ce/Zr. For the V/ZrCe$_x$ catalysts with different Ce/Zr ratios, the Hg^0 oxidation and NO conversions first increased and then decreased again as the Ce/Zr ratio increased. The V/ZrCe$_{0.6}$ catalyst exhibited the best Hg^0 oxidation and NO conversion. At 250 °C, Hg^0 oxidation efficiency and NO conversion was 77.6% and 87.3%, respectively. The possible reason was that the V/ZrCe$_{0.6}$ exhibited the largest BET surface area (as shown in Table 1) during the Ce/Zr ratios increasing from 0.2 to 1.0, which might affect the Hg^0 oxidation efficiency and NO conversions of V/ZrCe. Compared with the V/Zr catalysts, the addition of Ce widened the operating temperature window for the reaction as well as considerably improved catalytic performance (250–300 °C). It can be deduced that Ce added to V/Zr enhanced the catalytic activity and influenced the catalytic activity at low reaction temperatures. This owed to Zr–Ce mixed oxides, which was a key component for NH_3–SCR catalysts because of their favorable attributes, such as high temperature phase stability, good redox properties, and acidity [30]. Besides, according to the literature [31], the synergetic interaction between Ce and V species enhanced the reducibility of catalyst and thus improved the catalytic activity. Although the Hg^0 oxidation in SCR atmosphere was unsatisfactory, it is still encouraging because lower space velocity and the typical flue gas with HCl would result in higher Hg^0 oxidation efficiency.

Table 1
BET surface and pore parameters of the different catalysts.

Catalysts	BET surface area (m^2/g)	Pore volume (cm^3/g)	Average pore diameter (nm)
V/Zr	41.6	0.0745	7.16
V/Ce	41.3	0.0976	9.45
V/ZrCe$_{0.2}$	47.4	0.0445	3.75
V/ZrCe$_{0.4}$	48.7	0.0458	3.77
V/ZrCe$_{0.6}$	58.5	0.0708	4.84
V/ZrCe$_{0.8}$	56.7	0.0743	5.24
V/ZrCe$_{1.0}$	51.5	0.0728	5.65

3.1.2. Effect of Hg^0 on NO conversion

The main objective of this work was to achieve simultaneous removal of Hg^0 and NO using V/ZrCe catalysts. In real applications, gas-phase mercury is the typical components of flue gas. Thus, the effect of Hg^0 on NO conversion efficiency was studied. Based on the results in Fig. 3, NO conversion efficiency at different Hg^0 concentration exhibited similar trends. It was obvious that NO conversion efficiency increased with the increase of reaction temperature from 100 to 250 °C and then decreased slightly from 300 to 400 °C. Besides, NO conversion efficiency at different Hg^0 concentration was nearly the same to each other, which indicated that the addition of Hg^0 had little impact on NO conversion. It might be because the Hg^0 concentration (less than 140 μg/m^3) was extremely small compared to NO concentration (700 ppm).

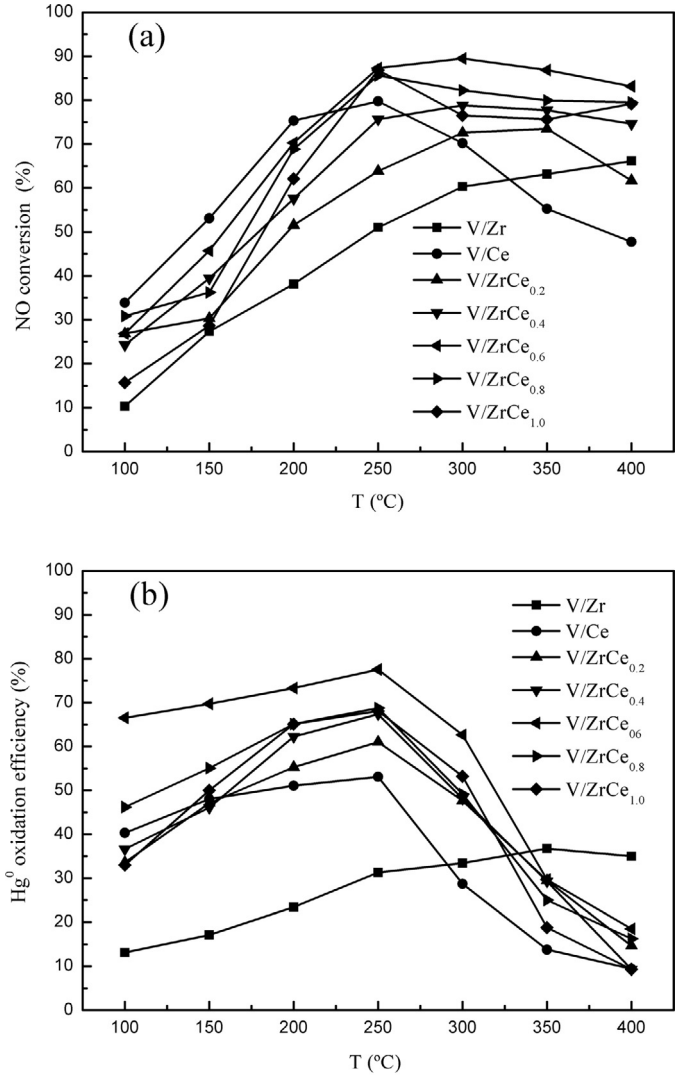

Fig. 2. Simultaneous removal of Hg^0 and NO on various catalysts in SCR atmosphere (NH_3/NO = 1). (Reaction condition: 70.0 μg/m^3 Hg^0, 700 ppm NO, NH_3/NO: 1, 6% O_2, 250 mg of sample, total flow rate 500 mL/min, GHSV 100,000 h^{-1}).

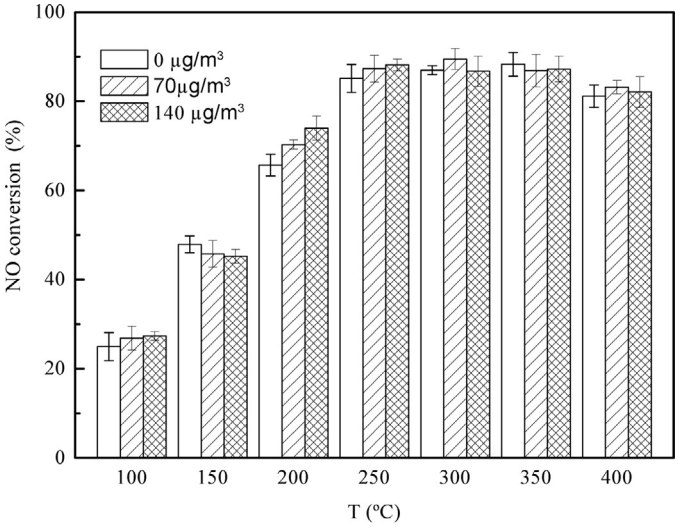

Fig. 3. Effects of Hg^0 on NO conversion efficiency. (Reaction condition: 0 ~ 140.00 μg/m^3 Hg^0, 700 ppm NO, NH_3/NO: 1, 6% O_2, 250 mg of sample, total flow rate 500 mL/min, GHSV 100,000 h^{-1}).

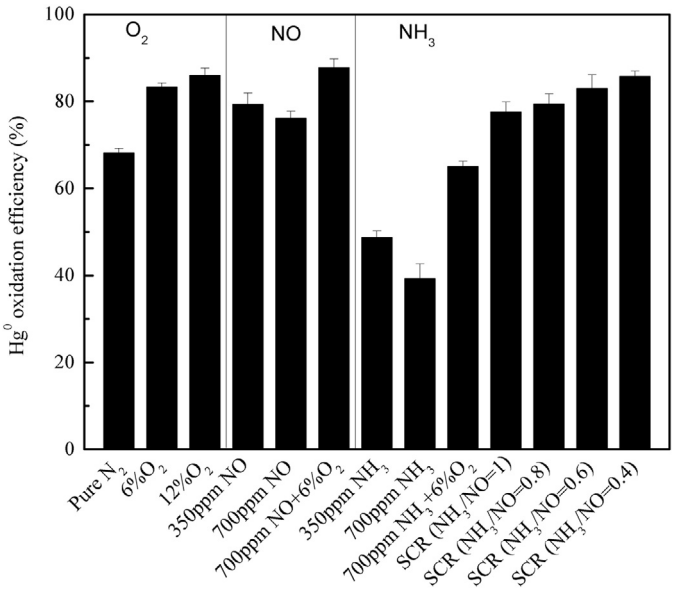

Fig. 4. Effects of SCR gas components on Hg^0 oxidation over V/$ZrCe_{0.6}$ catalysts at 250 °C. (Reaction condition: 70.00 μg/m^3 Hg^0, 0%–12%O_2; 0 ~ 700 ppm NO, 0 ~ 700 ppm NH_3, NH_3/NO: 0.4 ~ 1, 250 mg of sample, 500 mL/min total flow rate and GHSV 100000 h^{-1}).

3.1.3. *Effect of SCR gas components on Hg^0 oxidation*

3.1.3.1. Effect of O_2. Effects of SCR gas components on Hg^0 oxidation over the V/$ZrCe_{0.6}$ catalyst are summarized in Fig. 4. O_2 is critical for the oxidation of Hg^0. Hg^0 oxidation was observed to be 83.2% at 6% O_2, which was higher than the Hg^0 oxidation of 68.1% under pure N_2 gas flow. The loss of Hg^0 on the V/$ZrCe_{0.6}$ catalyst in pure N_2 atmosphere was due to the reaction between Hg^0 and the surface oxygen which could act as oxidants to sustain HgO formation on the surface of sample [32]. Based on the H_2-TPR and XPS results discussed later, the oxygen on the surface of the catalyst not only supplied abundant chemisorbed and lattice oxygen, but also enhanced the oxidation of NH_3 and the formation of highly reactive surface nitrates. Therefore, when 6% O_2 was introduced, gas-phase O_2 regenerated the lattice oxygen and replenished the chemisorbed oxygen, which facilitated Hg^0 oxidation. However, when O_2 concentration further increased to 12%, no obvious increase of Hg^0 oxidation was detected. This result suggested that 6% O_2 was sufficient for Hg^0 oxidation.

3.1.3.2. Effect of NO. The Hg^0 oxidation of the V/$ZrCe_{0.6}$ catalyst increased from 68.1% to 79.3% with the addition of 350 ppm NO. It indicated that the activity of V/$ZrCe_{0.6}$ catalyst for Hg^0 oxidation was enhanced with the presence of NO. This was probably because a fraction of NO reacted with the surface oxygen of catalyst to form NO_x species which can cause Hg^0 oxidation [33]. Besides, a Hg^0 oxidation of 76.1% was observed when NO concentration further increased to 700 ppm, which was still higher than that observed in pure N_2 atmosphere. However, 350 ppm and 700 ppm NO balanced in N_2 was lower than that observed under 6% O_2 atmosphere. It was hypothesized that part of the NO reaction consumed the surface oxygen which resulted in a slight decrease of Hg^0 oxidation. Hence, once 6% O_2 was added, gas-phase O_2 replenished the surface oxygen, which was sufficient for NO conversion and Hg^0 oxidation. Therefore, the coexistence of NO and O_2 would be beneficial for the Hg^0 oxidation.

3.1.3.3. Effect of NH_3. In this study, NH_3 is as a reducing agent in the SCR reaction. The V/ZrCe catalysts, which are developed for simultaneous removal of NO and Hg^0, would probably be used under SCR

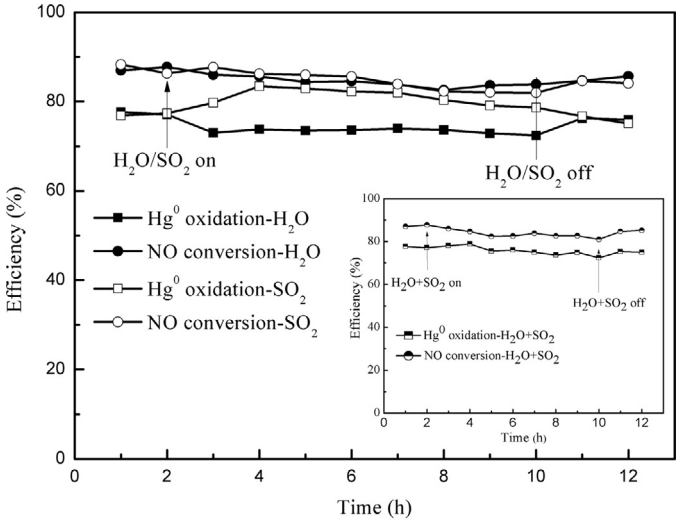

Fig. 5. The effect of H_2O and SO_2 on simultaneous removal of Hg^0 and NO over $V/ZrCe_{0.6}$ catalysts at 250 °C. (Reaction condition: 70.00 μg/m³ Hg^0, 700 ppm NO, NH_3/NO: 1, 6% O_2, 300 ppm SO_2 (when used), 8 vol.% H_2O (when used), 250 mg of sample, 500 mL/min total flow rate and GHSV 100,000 h^{-1}).

conditions where NH_3 is present. Therefore, it is necessary to study the effect of NH_3 on Hg^0 oxidation. 350 or 700 ppm of NH_3 was added into pure N_2 exhibited a significant inhibitive effect on Hg^0 oxidation. However, the Hg^0 oxidation efficiency increased from 39.3% to 65.0% when 6% O_2 was introduced into the gas flow containing 700 ppm NH_3. Some researchers [34,35] believe that the adsorbed NH_3 most probably reacted with the surface oxygen to form NH_2 and OH. The reaction process is as follows:

$$NH_3(g) \rightarrow NH_3(ad) \quad (3)$$

$$NH_3(ad)+O^*(ad) \rightarrow NH_2(ad)+OH(ad) \quad (4)$$

where O* is active surface oxygen of catalyst. The consumption of surface oxygen by NH_3 was mostly responsible for the decrease of Hg^0 oxidation. The presence of gas-phase O_2 could offsets the greater part of the inhibitive effect of NH_3 because the consumption of surface oxygen can be replenished. Besides, the effect of NH_3/NO ratio on Hg^0 oxidation was also investigated. The Hg^0 oxidation efficiency increased from 77.6% to 85.7% with the decrease of NH_3/NO ratio from 1.0 to 0.4. It would be deduced that the SCR reaction consumed NH_3, which could offsets a part of the inhibitive effect of NH_3 on Hg^0 oxidation. Furthermore, the surplus NO should facilitate Hg^0 oxidation when the NH_3/NO ratio was smaller than 1.0 [36]. In general, Hg^0 oxidation was inhibited in SCR atmosphere owing to the presence of NH_3. Nevertheless, it is still an inspiring Hg^0 oxidation in typical flue gas with HCl.

3.1.4. Effect of H_2O and SO_2 on simultaneous removal of NO and Hg^0

Because the combustion exhaust contains water vapor and SO_2 in practical applications, the influence of H_2O/SO_2 on the activity over $V/ZrCe_{0.6}$ catalyst was investigated. As shown in Fig. 5, the addition of 8 vol.% H_2O had a negligible inhibition effect on NO conversion and Hg^0 oxidation. The Hg^0 oxidation and NO conversion remained above 72.9% and 82.6% respectively for the entire 8 h, suggesting that $V/ZrCe_{0.6}$ catalyst exhibited strong resistance to H_2O poisoning at 250 °C. The effect of 300 ppm SO_2 over $V/ZrCe_{0.6}$ catalysts activity is also shown in Fig. 5. The NO conversion showed a slight decline over time and decreased to 82.0% when SO_2 was introduced into the reaction atmosphere. After removing SO_2, the NO conversion was partially restored. This result indicated that SO_2 inhibited the catalytic activity slightly at 250 °C, which may be attributed to the deposition of ammonium sulfate/bisulfate on the surface. It is interesting to note that Hg^0 oxidation efficiency was first increased and then slightly decreased over time in the presence of SO_2. This indicated that promotional effect of SO_2 on Hg^0 oxidation was obtained. It was very likely that SO_2 reacted with the surface oxygen to form SO_3 that were responsible for the enhanced Hg^0 oxidation [37]. A promotional effect of SO_2 on Hg^0 oxidation is presented as follow:

$$SO_2 + \frac{1}{2}O_2 \rightarrow SO_3 \quad (5)$$

$$Hg^0 + \frac{1}{2}O_2 + SO_3 \rightarrow HgSO_4 \quad (6)$$

Fig. 5 (inset) shows the influence of H_2O and SO_2 on the catalytic performance of catalyst. When 8 vol.% H_2O and 300 ppm SO_2 were added into the SCR atmosphere (NH_3/NO = 1), a slight decline of the NO conversion was observed over time. The Hg^0 oxidation did not show any decrease for the first 2 h. However, further increasing the reaction time resulted in a slight decline of Hg^0 oxidation and decreased to 72.4%. It might be because H_2SO_4 can form when SO_2, O_2, and H_2O co-exist, which will likely affect the behavior of Hg^0 on the surface of catalyst [37]. Then the H_2SO_4 reacted with HgO to form $HgSO_4$. After the removal of SO_2 and H_2O, the catalytic activity recovered but not returned to the original level yet. It implied that the ammonium sulfate/bisulfate which blocked the active sites led to a slight decrease of catalytic activity. However, the catalytic activity was still maintained at a relatively high level during the measured period. Combined with the result of upper experiment, the $V/ZrCe_{0.6}$ catalyst has excellent H_2O and SO_2 durability, which is very competitive for practical application on simultaneous removal of NO and Hg^0.

3.2. Structural properties

3.2.1. BET

The BET specific surface area, pore volume and pore size of the catalysts are shown in Table 1. The BET surface area of $V/ZrCe_x$ was larger than that of V/Zr and V/Ce. Besides, with increasing the molar ratio of Ce/Zr, a marked increase in the BET surface area was observed. In particular, $V/ZrCe_{0.6}$ catalyst displayed the largest surface area, which was in consistent with the best catalytic performance. The material owning higher BET specific surface area could provide more surface active sites for the reactants [38,39], by which the catalytic activity could be promoted. Besides, it was concluded that some synergistic effect must exist between the Ce and Zr oxide species. The $V/ZrCe_x$ catalysts with higher surface area may be attributed to a transformation of the bulk, regular crystals to an amorphous or crystallite structure during co-precipitation, as shown by XRD. Meanwhile, the amorphous or crystallite structure usually has a higher surface area than the crystallized structure [40].

3.2.2. XRD and SEM

Fig. 6 shows the XRD patterns and the SEM images of the prepared samples. To identify the crystal structures of catalysts, XRD was characterized. As shown in Fig. 6(a), the main peaks of V/Ce in the diffraction profiles can be attributed to CeO_2 with the cubic fluorite structure (PDF-ICDD 43–1002) [4]. The diffraction peaks of the V/Zr showed monoclinic ZrO_2 (PDF-ICDD 36–0420) [41]. For the $V/ZrCe_x$ catalysts, the diffraction peaks were obviously attributed to the cubic fluorite structure of $CeZrO_4$ (PDF-ICDD 54-0017), indicating that the CeO_2–ZrO_2 solid solution was formed [42]. Interestingly, no XRD lines corresponding to crystalline vanadia were noted. It can be assumed that the impregnated vanadium oxide was in a highly dispersed or amorphous state on the surface of the support. Besides, full width at half maximum (FWHM)

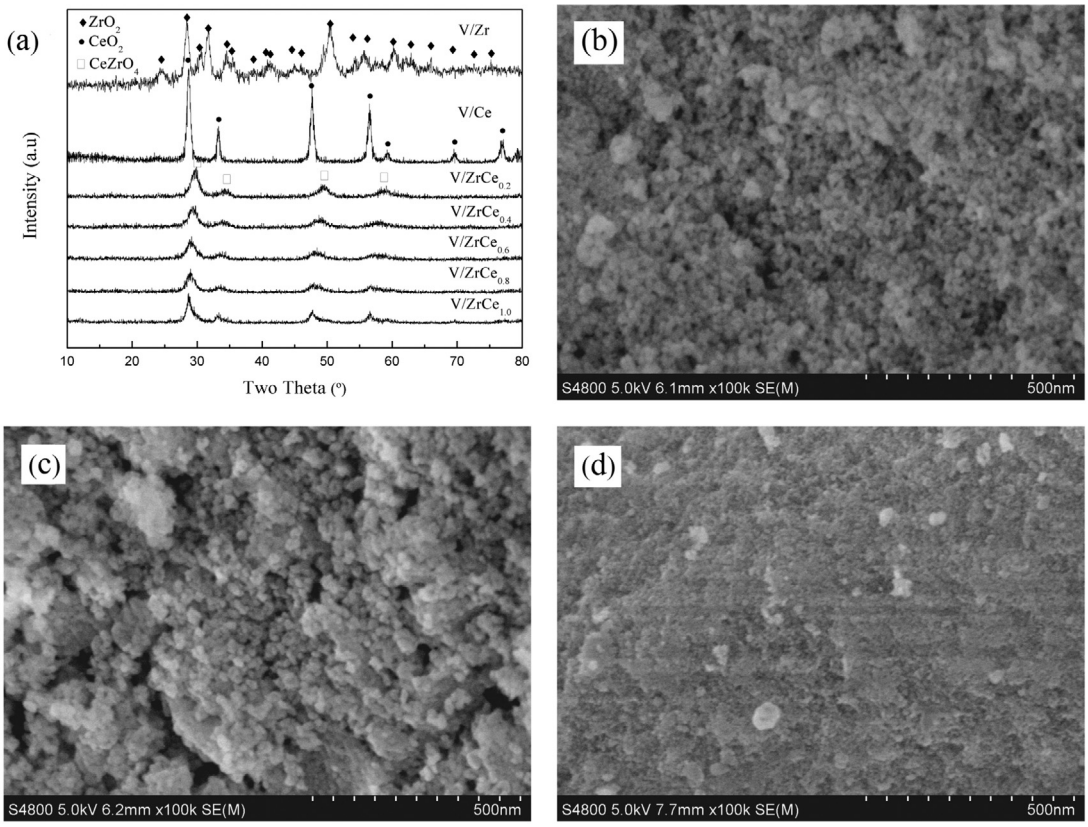

Fig. 6. (a) XRD patterns of various catalysts; SEM photographs of (b) V/Ce, (c) V/Zr, (d) V/$ZrCe_{0.6}$.

enlarges and the peak intensity decreased on V/$ZrCe_x$ catalysts. This indicated that the formation of CeO_2–ZrO_2 solid solution affected the structure of the catalyst, and it weakened the crystallinity and reduced the crystalline size. It was reported that amorphous or crystallite materials with enormous structure distortion would provide more active sites for catalytic reactions than crystalline materials, which was probably responsible for the high catalytic activity [43]. These results also indicated that the $ZrCe_x$ support was beneficial for the dispersion of active components and resulted in high NO conversion and Hg^0 oxidation.

SEM studies were conducted to investigate the surface morphology of the catalysts. As displayed in Fig. 6(b)–(d), the nanoparticles of the V/Ce evenly dispersed without agglomeration, whereas the agglomeration was observed over the V/Zr catalyst. The particle size of V/$ZrCe_{0.6}$ catalysts observed with SEM was smaller than that of V/Zr and V/Ce, which could be due to the interaction between Ce and Zr during preparation process of V/$ZrCe_{0.6}$ catalyst. The SEM image of V/$ZrCe_{0.6}$ catalysts at high magnification showed homogeneous distribution of nanoparticles with an average size of around 5–25 nm. Such results indicated that Ce can prevent the aggregation of Zr particles. Combined with the BET and XRD results, it could be inferred that the combination of Ce and Zr significantly affected texture properties of catalysts, which played an important role in catalytic activity.

3.2.3. NH_3-TPD

The NH_3-TPD curves for various catalysts are shown in Fig. 7. After deconvoluting, three main ammonia desorption peaks was observed over the entire desorption temperature range. A small peak was located at 159.4–191.2 °C, and two large ammonia desorption peaks were located at 225.6-250.7 °C and 295.7–340.7 °C, respectively. According to the literatures [23,38,44,45], the peak at 159.4–191.2 °C should be assigned to NH_3 desorbed by the weak acid sites; the peak at 225.6–250.7 °C was ascribed to the desorption of coordinated NH_3 bound to Brønsted acid sites; the peak at 295.7–340.7 °C was ascribed to the desorption of coordinated NH_3 bound to the Lewis acid sites. Compared with the V/Zr catalysts, the addition of Ce caused broadening of desorption peak. Besides, V/$ZrCe_{0.2}$ had the smallest desorption peak, the intensity of desorption peak enhanced with the Ce/Zr ratio varying from 0.2 to 0.6. However, the intensity declined with further increasing Ce/Zr ratio. V/$ZrCe_{0.6}$ had the biggest desorption peak area, denoting that it had the most acid amount. Combined with the BET results, the biggest desorption peak area of V/$ZrCe_{0.6}$ may be caused by the biggest surface area.

3.3. Redox properties

3.3.1. H_2-TPR

As illustrated in Fig. 8, H_2-TPR analysis was conducted to study the redox property of V/Zr, V/Ce and V/$ZrCe_{0.6}$ catalysts. Some researchers reported that pure ZrO_2 does not show any reduction peak below 900 °C [42,46]. Therefore, V/Zr catalysts showed a major broad peak with maximum at 456 °C, which can be likely corresponded to the reduction of V^{5+} to V^{3+} [22]. V/Ce exhibited the reduction peaks at around 550 °C, which was assigned to the reduction of surface oxygen [4]. And the noticeable and broad shoulder peak at 716 °C was ascribed to the reduction of lattice oxygen [4]. The peaks of V/$ZrCe_{0.6}$ at 580 °C were assigned to the reduction of ceria–zirconia mixed oxides [47,48]. Meanwhile, it can be seen that the peak area of V/$ZrCe_{0.6}$ was larger than that of V/Zr and V/Ce catalyst, which indicated that redox ability of V/$ZrCe_{0.6}$ was greatly improved. Higher redox ability of V/$ZrCe_{0.6}$ could enhance the mobility of surface oxygen due to the strong synergetic effect among Zr, Ce and V species. It was believed that the synergetic effect led to severe structural distortion and affluent oxygen defects

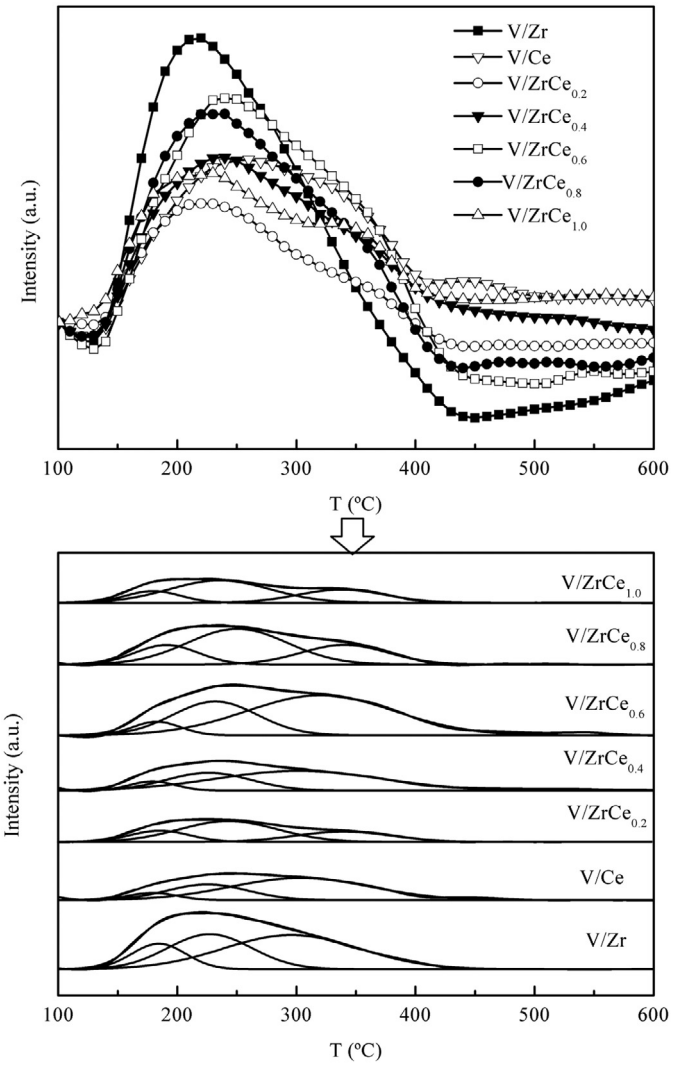

Fig. 7. NH_3-TPD profiles of V/ZrCe catalysts.

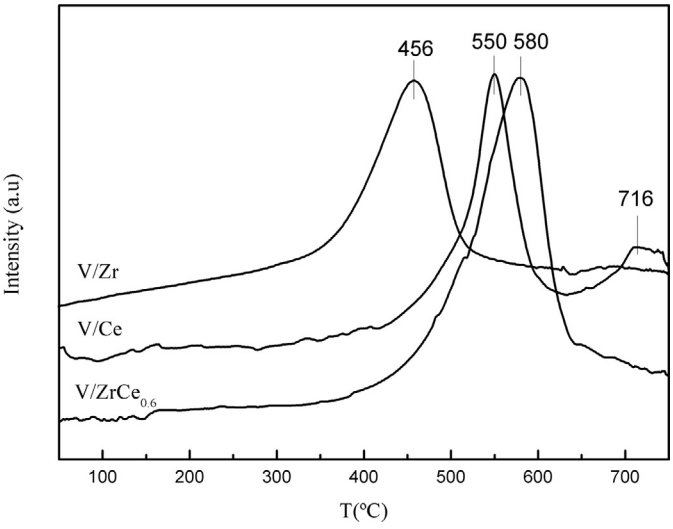

Fig. 8. H_2-TPR profiles of various catalysts.

[49,50]. Combined with the results of XPS, the good reducibility owing to the increase of the amount and the kinds of reactive oxygen species, can provide a facile redox process that would contribute to enhancing the catalytic activity [51].

3.3.2. XPS

XPS measurements were carried out over the fresh and used $V/ZrCe_{0.6}$ catalyst to provide information about the surface interaction and the chemical state of elements on the surface of catalysts. The used $V/ZrCe_{0.6}$ catalyst was carried out on the fixed bed reaction system under SCR atmosphere with or without SO_2 at 250 °C. As shown in Fig. 9(a), the O 1s peak was fitted into two sub-bands: the peak at around 529.2–530.3 eV was attributed to the lattice oxygen O^{2-} (denoted as (Oβ)), while the one at around 531.3–532.3 eV corresponded to the chemisorbed oxygen (denoted as (Oα)) such as O_2^{2-} or O^- [52]. However, O 1 s of V/Ce and V/Zr shifted to the low binding energy direction. Besides, the binding energy (BE) value of the V/Ce catalyst was lower than those of the V/Zr and $V/ZrCe_{0.6}$ catalysts, showing that Ce donated more electrons to oxygen species. The BE of Oβ peaks tended to shift towards higher BE (approximately 1.0 eV) over $V/ZrCe_{0.6}$ catalysts, which was related to the partial conversion of Ce^{4+} into Ce^{3+} species [53]. The ratio of Oβ, calculated by Oβ/(Oα + Oβ), over $V/ZrCe_{0.6}$ (36.9%) was higher than that over V/Ce (30.6%) and V/Zr (24.0%), demonstrating that the amount of lattice oxygen species on $V/ZrCe_{0.6}$ catalysts was increased. Oxygen species can be stored/released by ceria via the redox shift between Ce^{4+}/Ce^{3+} [54], leading to the increase of surface mobile oxygen, which was beneficial to the redox properties.

Fig. 9(b) depicts the XPS spectra in the V 2p region for the $V/ZrCe_{0.6}$ catalysts. Two peaks at 518.0 and 519.8 eV for the fresh $V/ZrCe_{0.6}$ catalysts corresponded to the oxidation states V^{4+} and V^{5+}, respectively [55]. Binding energy of V^{5+} on catalyst surface increased after the reaction without SO_2, while binding energy of V^{4+} slightly decreased, suggesting that some V^{5+} was reduced toV^{4+} [56]. Furthermore, the V^{5+}/V^{4+} ratio decreased from 1.2 to 1.0, which also indicated that V^{4+} species increased after reaction without SO_2. According to the previous studies [16], Hg^0 in flue gas can react with V_2O_5 on catalyst surface and then form V^{4+} species and HgO. That was the reason why V^{4+} content increased. It's worth noting that the catalysts were found to be reported for V^{3+} (514.5 eV), V^{4+} (516.4 eV) and V^{5+} (518.3 eV) after the reaction with SO_2. Dunn et al. [57] proposed that SO_2 oxidation to SO_3 occurs on V_2O_5, and at the same time the valence of V^{5+} ions changes to V^{3+}. However, the content of V^{5+} has remained fairly constant compared to the fresh catalyst. The catalyst would maintain excellent catalytic performance for relative long time. This could be because V^{5+} were re-oxidized by oxygen molecules ($O_{2(g)}$) or adsorbed oxygen species on the surface (O_{ad}) [58]. In addition, we found that the conversion of SO_2 to SO_3 over V/ZrCe catalyst was less than 1% during the experiment, which was negligible. SO_3 could react with Hg^0 to produce $HgSO_4$. The reactions could be described as:

$$SO_2 + V^{5+}\text{-O-} \rightarrow SO_3 + V^{3+} \quad (7)$$

$$V^{3+} + \left(\frac{1}{2}O_2(g) \text{or } O_{ad}\right) \rightarrow V^{5+}\text{-O-} \quad (8)$$

The XPS results of Ce 3d for $V/ZrCe_{0.6}$ are shown in Fig. 9(c). The bands labeled u, u″, u‴, v, v″ and v‴ are assigned to Ce^{4+}, whereas the peaks labeled u′ and v′ are ascribed to Ce^{3+} ions. It was evident that the coexistence of Ce^{4+} and Ce^{3+} over the fresh $V/ZrCe_{0.6}$ catalysts offered the possibility of oxygen storage and release, which enhanced the catalyst activity. Based on the peak areas, Ce^{4+} oxide was the primary form, which was considered to be beneficial for the oxidation reactions [59]. The presence of Ce^{3+} could create charge imbalance, the vacancies and unsaturated chemical bonds on the catalyst surface, leading to more surface oxygen species formed

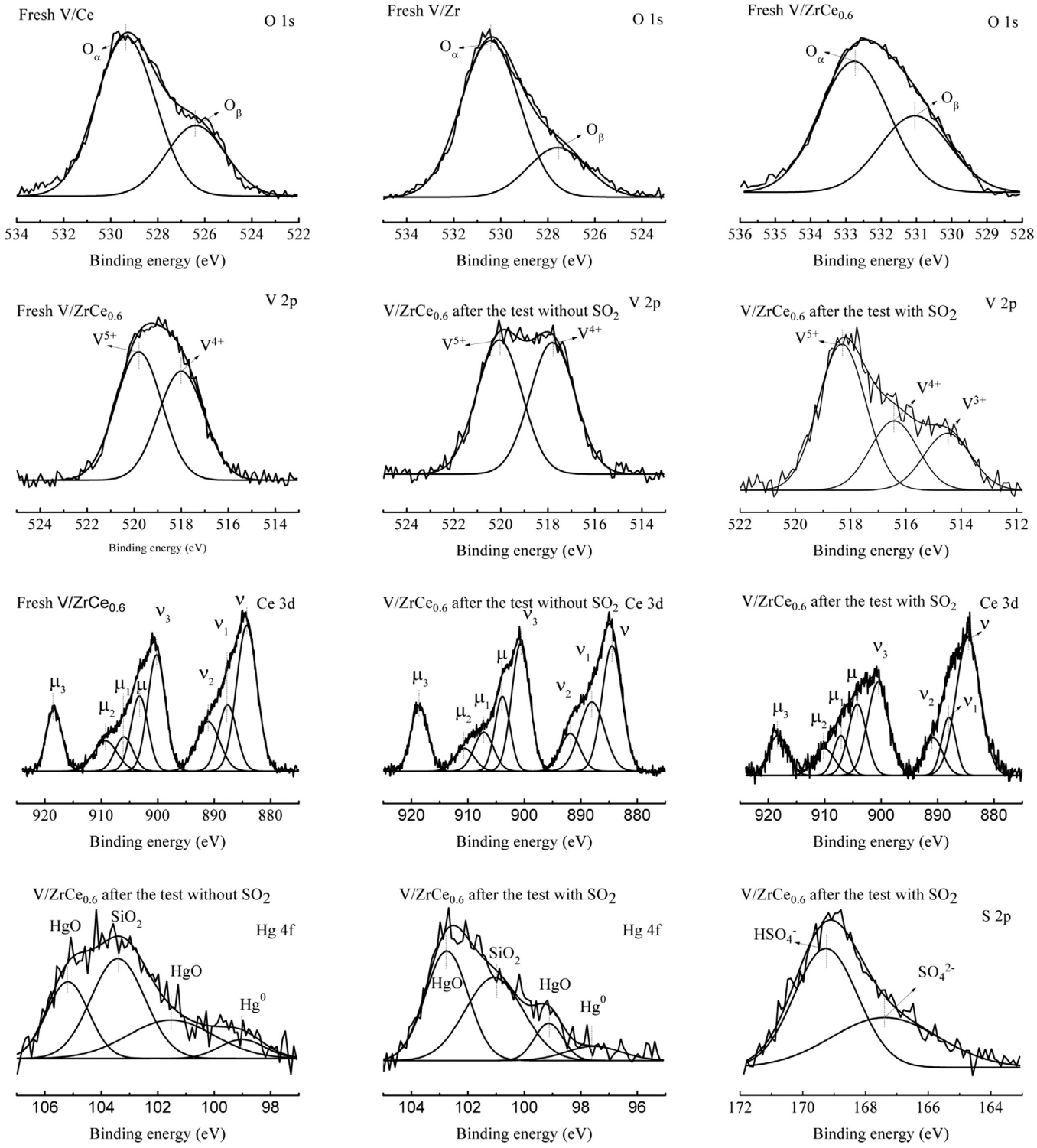

Fig. 9. XPS spectra of the catalysts over the spectral regions of Ce 3d, V 2p and O 1 s before the test, and Ce 3d, V 2p, Hg 4f, and S 2p after the test with or without SO_2 (Reaction condition: 70.00 μg/m^3 Hg^0, 700 ppm NO, NH_3/NO: 1, 6% O_2, 0/300 ppm SO_2, 250 mg of sample, 500 mL/min total flow rate and GHSV 100,000 h^{-1}).

[60]. Combined with results of XRD, XRD patterns did not exhibit extra peaks, indicating no phase segregation occurred. Liu et al. [61] found that the enhancement of homogeneous Ce and Zr atoms could ease the valence change of Ce ($Ce^{4+} \rightarrow Ce^{3+}$). After the reaction without SO_2, the ratio of Ce^{4+}/Ce^{3+} decreased from 5.0 to 3.3 compared to the fresh catalyst, indicating that some Ce^{4+} was reduced to Ce^{3+} during the reaction. The generation of V^{4+} together with Ce^{3+} is indicative of the redox equilibrium ($Ce^{3+} + V^{5+} \leftrightarrow Ce^{4+} + V^{4+}$). The redox couple Ce^{4+}/Ce^{3+} could transfer electrons to V^{5+}, which was the enhancement of reduced vanadium species. The ratio of Ce^{4+}/Ce^{3+} increased to 6.1 after the reaction with SO_2, which may be due to the oxidation of Ce^{3+} by O_2 in the presence of SO_2.

Hg^0 oxidation by V/$ZrCe_{0.6}$ catalysts may be attributed to the Mars-Maessen mechanism [62,63]. The Hg 4f XPS patterns are shown in Fig. 9(d). The characteristic peak at 99.0 eV was ascribed to Hg^0 [64]. The peak at 101.3and 105.2 eV corresponded to Hg 4f

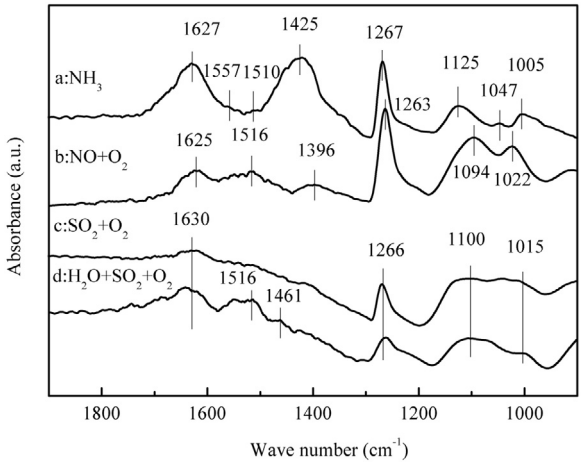

Fig. 10. FT-IR spectra taken upon V/ZrCe$_{0.6}$ catalysts.

7/2 and Hg 4f 5/2, respectively, and were assigned to HgO [65,66]. The peak at 103.4 eV was attributed to Si 2p of SiO_2 in quartz wool [65]. This indicated that the main species of mercury was HgO on the surface of V/ZrCe$_{0.6}$ after the test without SO_2. The adsorption of Hg^0 occurred on the surfaces of V/ZrCe$_{0.6}$ catalysts followed by a subsequent heterogeneous oxidative transformation of Hg^0 to HgO by reactive surface oxidants [62]. At the same time, the Hg 4f peaks of V/ZrCe$_{0.6}$ after the test with SO_2 shifted to the low binding energy direction, which centered at about 99.1 and 102.8 eV. Combined with the XPS results in the S 2p region, the results were further confirmed that the oxidized mercury may transform to $HgSO_4$ in the presence of SO_2. The S 2p peaks mainly centered at 167.4 and 169.3 eV, which may be ascribed to SO_4^{2-} and HSO_4^-, respectively [67]. During the reaction, the formation of SO_4^{2-} was also supported by the spectra of V 2p region.

3.4. FT-IR characterization: study of NH_3 and NO_x adsorption abilities and influence of H_2O and SO_2

The FT-IR spectra of V/ZrCe$_{0.6}$ catalyst at different gases for 60 min are showed in Fig. 10. As shown in Fig. 10a, several bands attributed to different form of NH_3 molecule were observed on the catalyst surface. The bands at 1005 cm^{-1}, 1047 cm^{-1}, 1125 cm^{-1}, 1267 cm^{-1} and 1627 cm^{-1} can be attributed to asymmetric and symmetric bending vibrations of NH_3 coordinated on Lewis acid sites [34,68], while the band at 1425 cm^{-1} can be assigned to asymmetric and symmetric bending vibrations of NH_4^+ species on Brønsted acid sites [25,69,70]. The band at 1510 cm^{-1} and 1557 cm^{-1} were assigned to amide species (-NH_2) [68]. This indicated that the V_2O_5 had an ability to oxidize (or dehydrogenize) NH_3 into NH_2, which was considered as the intermediate of the SCR reaction [71,72]. Fig. 10b shows the FT-IR spectra results of NO_x adsorption over V/ZrCe$_{0.6}$ catalysts. After NO + O_2 adsorption, several weak bands were detected at 1022, 1094, 1263, 1396, 1516 and 1625 cm^{-1}. The bands at 1022 and 1094 cm^{-1} were attributed to anionic nitrosyl NO− species, which can be oxidized to nitrate or nitrite species in the presence of oxygen [73]. The bands at 1263 and 1625 cm^{-1} were ascribed to bridging nitrate [74], while the band at 1396 cm^{-1} can be attributed to M-NO_2 nitro compounds [75]. Besides, a series of successive peaks in the range of 1500–1580 cm^{-1} could be assigned to NO_2-containing species, like nitrito (O-bound NO_2) and nitrato (NO_3) species [76]. Some researchers [77,78] demonstrated that the adsorbed nitrates species could participate in the redox reaction sufficiently. At the same time, the FT-IR spectra of SO_2 and H_2O adsorption were also conducted. As shown in Fig. 10c, several bands at 1630, 1266, 1100, and 1015 cm^{-1} were detected on the catalyst. The band at 1630 cm^{-1} was assigned to δ_{HOH} of H_2O, suggesting that surface water was formed [79]. Three absorption bands between 1000 and 1300 cm^{-1} were also discernible on the catalysts, suggesting that the bidentate sulfates formed [80,81]. Chang et al. [81,82] held the opinion that the bidentate sulfate could provide new acid sites for NH_3 adsorption and the emerging sites were mainly Lewis acid sites. Moreover, the formation of bidentate sulfate would greatly increase the amount of NH_4^+ [83]. These would alleviate the inhibition of ammonium sulfate/bisulfate deposition on the catalyst. It is noteworthy that similar bands also appeared after $H_2O + SO_2 + O_2$ treatment. The major difference was that two new absorption bands at 1516 and 1461 cm^{-1} appeared when SO_2, O_2, and H_2O co-exist. These bands were attributed to the vibrations of the surface hydroxyl species (OH), demonstrating that gaseous H_2O and O_2 were prone to forming active oxygen and hydroxyl on the surface [80].

3.5. Mechanism discussion

From the above studies, the reaction over the surface of V/ZrCe$_{0.6}$ catalysts included both Hg^0 oxidation and NO conversion. The cerium can occupy two oxidation states [CeO_2 (Ce^{4+}) ↔ Ce_2O_3 (Ce^{3+})], allowing ceria from the CeO_2–ZrO_2 support to accommodate more surface lattice oxygen species. The existence of redox equilibrium ($Ce^{3+} + V^{5+} \leftrightarrow Ce^{4+} + V^{4+}$) could be beneficial to the NH_3-SCR reaction and Hg^0 oxidation. On one hand, combining the results obtained in this study and the literature [84], Hg^0 oxidation mainly occurs via a Mars–Maessen mechanism. Hg^0 (g) firstly absorbed on the surface of the catalysts to form Hg(ad), then V_2O_5 and CeO_2 offered the lattice oxygen for the oxidation of Hg(ad). The reduced V_2O_4 and Ce_2O_3 can be converted back to their original state by O_2 in the gas. The redox equilibrium enhanced the reducibleness of vanadia species. In addition, SO_2 participated in the Hg^0 oxidation reaction and $HgSO_4$ was generated. NO could be oxidized into NO_2 by surface oxygen, and NO_2 could react with Hg^0 to form $Hg(NO_3)_2$. The oxidation mechanism of Hg^0 can be described as follows:

$$Hg^0{}_g \rightarrow Hg^0{}_{ad} \quad (9)$$

$$Hg^0{}_{ad} + O_\beta \rightarrow HgO_{ad} \quad (10)$$

$$V_2O_5 \rightarrow V_2O_4 + O_\beta \quad (11)$$

$$2CeO_2 \rightarrow Ce_2O_3 + O_\beta \quad (12)$$

$$V_2O_4 + \frac{1}{2}O_{2(g)} \rightarrow V_2O_5 \quad (13)$$

$$Ce_2O_3 + \frac{1}{2}O_{2(g)} \rightarrow 2CeO_2 \quad (14)$$

$$V_2O_5 + Ce_2O_3 \leftrightarrow V_2O_4 + 2CeO_2 \quad (15)$$

On the other hand, Both Lewis and Brønsted acid sites exist on the surface of V/ZrCe$_{0.6}$ catalysts, leading to the appearance of coordinated NH_3, NH_4^+, —NH_2 and other intermediates from NH_3 oxidation. NO can be oxidized to NO_2 and intermediate nitrate on the catalyst surface in the presence of oxygen. The adsorbed NH_3 or NH_4^+ would react with the NO_2 species generated at the surface to form intermediate species, which further react with gaseous NO or adsorbed NO to form N_2. Furthermore, —NH_2 could react with NO to form N_2. Based on the XPS and FT-IR spectroscopic results as well as the earlier reports [68,85], the possible mechanism for the SCR reaction of NO by NH_3 can be facilitated as follows:

$$O_{2(g)} \rightarrow O^*(ad) \quad (16)$$

$$NH_3(g) \rightarrow NH_4^+(ad) \quad (17)$$

$$2NO(g) + O_2(g) \rightarrow 2NO_2(ad) \quad (18)$$

$$2NH_3(ad)+NO_2(ad)+NO(g) \rightarrow 2N_2+3H_2O \quad (19)$$

$$2NH_4^+(ad)+NO_2(ad)+NO(g) \rightarrow 2N_2+3H_2O+2H^+ \quad (20)$$

$$NO(ad)+NH_2(ad) \rightarrow NH_2NO(ad) \rightarrow N_2(g)+H_2O(g) \quad (21)$$

4. Conclusions

A series of $V/ZrCe_x$ catalyst was prepared by a co-precipitation method for simultaneous removal of NO and Hg^0. $V/ZrCe_{0.6}$ exhibited superior NO conversion (87.3%) and Hg^0 oxidation efficiency (77.6%) in SCR atmosphere ($NH_3/NO=1$) at 250 °C. The catalyst also exhibited a better SO_2 and H_2O durability due to the formed of bidentate sulfates. The addition of Hg^0 had little impact on NO conversion because of the smaller Hg^0 concentration. NH_3 consumed the surface oxygen, hence inhibiting Hg^0 oxidation. However, gas-phase O_2 regenerated the lattice oxygen and replenished the chemisorbed oxygen, which facilitated Hg^0 oxidation. NO and SO_2 had a promoting effect on Hg^0 oxidation in the presence of O_2. In addition, the characterization results showed that the features of $V/ZrCe_{0.6}$, such as lower crystallinity, better texture properties, strong redox ability and high reactive nitrate together with NH_3 species, were favorable for the superior catalytic performance. The redox equilibrium ($Ce^{3+}+V^{5+} \leftrightarrow Ce^{4+}+V^{4+}$) was beneficial to the Hg^0 oxidation and NO conversion. Based on the results, the catalytic mechanism for simultaneous removal of Hg^0 and NO over V_2O_5/ZrO_2–CeO_2 was proposed: $2NH_3/NH_4^+(ad)+NO_2(ad)+NO(g) \rightarrow 2N_2+3H_2O+/2H^+$, $Hg(ad)+O\beta \rightarrow HgO(ad)$.

Acknowledgments

This project was financially supported by the National Natural Science Foundation of China (51278177, 51478173), and the Scientific and Technological Major Special Project of Changsha City in China (k1502028-31).

References

[1] Y. Wang, B. Shen, C. He, S. Yue, F. Wang, Environ. Sci. Technol. 49 (2015) 9355–9363.
[2] C. Su, X. Ran, J. Hu, C. Shao, Environ. Sci. Technol. 47 (2013) 11562–11568.
[3] Y. Zhao, R. Hao, B. Yuan, J. Jiang, J. Hazard. Mater. 301 (2016) 74–83.
[4] Z. Lian, F. Liu, H. He, Ind. Eng. Chem. Res. 53 (2014) 19506–19511.
[5] Y. Zhao, R. Hao, M. Qi, Chem. Eng. J. 269 (2015) 159–167.
[6] Y. Yuan, J.Y. Zhang, H.L. Li, Y. Li, Y.C. Zhao, C.G. Zheng, Chem. Eng. J. 192 (2012) 21–28.
[7] R. Liu, W. Xu, L. Tong, T. Zhu, J. Environ. Sci. 38 (2016) 126–132.
[8] P. Fang, C.P. Cen, X.M. Wang, Z.J. Tang, Z.X. Tang, D.S. Chen, Fuel. Process. Technol. 106 (2013) 645–653.
[9] U.S. Environmental Protection Agency, Air Toxics Standards for Utilities, http://www.epa.gov/ttn/atw/utility/utilitypg.html.
[10] F. Xu, Z. Luo, W. Cao, P. Wang, B. Wei, X. Gao, M. Fang, K. Cen, J. Environ. Sci. 21 (2009) 328–332.
[11] A. Karami, V. Salehi, J. Catal. 292 (2012) 32–43.
[12] M. Rallo, M.A. Lopez-Anton, M.L. Contreras, M.M. Maroto-Valer, Environ. Sci. Pollut. Res. 19 (2012) 1084–1096.
[13] S. Sjostrom, M. Durham, C.J. Bustard, C. Martin, Fuel 89 (2010) 1320–1322.
[14] C. He, B. Shen, J. Chen, J. Cai, Environ. Sci. Technol. 48 (2014) 7891–7898.
[15] N. Fernández-Miranda, M.A. Lopez-Anton, M. Díaz-Somoano, M.R. Martínez-Tarazona, Chem. Eng. J. 285 (2016) 77–82.
[16] L. Zhao, C. Li, J. Zhang, X. Zhang, F. Zhan, J. Ma, Y.e. Xie, G. Zeng, Fuel 153 (2015) 361–369.
[17] H. Chang, Q. Wu, T. Zhang, M. Li, X. Sun, J. Li, L. Duan, J. Hao, Environ. Sci. Technol. 49 (2015) 12388–12394.
[18] J. He, G.K. Reddy, S.W. Thiel, P.G. Smirniotis, N.G. Pinto, Energy Fuel. 27 (2013) 4832–4839.
[19] X. Zhang, C. Li, L. Zhao, J. Zhang, G. Zeng, Appl. Surf. Sci. 347 (2015) 392–400.
[20] B.M. Reddy, P. Lakshmanan, A. Khan, J. Phys. Chem. B 108 (2004) 16855–16863.
[21] Y. Zhang, W. Guo, L. Wang, M. Song, L. Yang, K. Shen, H. Xu, C. Zhou, Chin. J. Catal. 36 (2015) 1701–1710.
[22] S. Putluru, A. Riisager, R. Fehrmann, Catal. Lett. 133 (2009) 370–375.
[23] Z. Ma, X. Wu, Z. Si, D. Weng, J. Ma, T. Xu, Appl. Catal. B: Environ. 179 (2015) 380–394.
[24] Z. Liu, S. Zhang, J. Li, J. Zhu, L. Ma, Appl. Catal. B: Environ. 158 (2014) 11–19.
[25] S. Ding, F. Liu, X. Shi, H. He, Appl. Catal. B: Environ. 180 (2016) 766–774.
[26] B. Shen, Y. Wang, F. Wang, T. Liu, Chem. Eng. J. 236 (2014) 171–180.
[27] H. Li, C.Y. Wu, Y. Li, J. Zhang, Appl. Catal. B: Environ. 111–112 (2012) 381–388.
[28] A. Zhang, W. Zheng, J. Song, S. Hu, Z. Liu, J. Xiang, Chem. Eng. J. 236 (2014) 29–38.
[29] H.L. Li, C.Y. Wu, Y. Li, J.Y. Zhang, Environ. Sci. Technol. 45 (2011) 7394–7400.
[30] N. Marcotte, B. Coq, C. Savill-Jovitt, P. Bichon, R. Cavalier, R. Durand, V. Harle, R. Marques, E. Rohart, Appl. Catal. B: Environ. 105 (2011) 373–376.
[31] Z. Ma, X. Wu, Y. Feng, Z. Si, D. Weng, L. Shi, Prog. Nat. Sci. 25 (2015) 342–352.
[32] S. Tao, C. Li, X. Fan, G. Zeng, P. Lu, X. Zhang, Q. Wen, W. Zhao, D. Luo, C. Fan, Chem. Eng. J. 210 (2012) 547–556.
[33] Y. Li, P.D. Murphy, C.Y. Wu, K.W. Powers, J.C.J. Bonzongo, Environ. Sci. Technol. 42 (2008) 5304–5309.
[34] G. Qi, R.T. Yang, R. Chang, Appl. Catal. B: Environ. 51 (2004) 93–106.
[35] J. Zhou, W. Hou, P. Qi, X. Gao, Z. Luo, K. Cen, Environ. Sci. Technol. 47 (2013) 10056–10062.
[36] H. Li, S. Wu, C.-Y. Wu, J. Wang, L. Li, K. Shih, Environ. Sci. Technol. 49 (2015) 7373–7379.
[37] L. Zhao, C. Li, X. Zhang, G. Zeng, J. Zhang, Y.e. Xie, Environ. Sci. Pollut. Res. 23 (2016) 1471–1481.
[38] T. Zhang, R. Qu, W. Su, J. Li, Appl. Catal. B: Environ. 176–177 (2015) 338–346.
[39] Z. Wu, R. Jin, Y. Liu, H. Wang, Catal. Commun. 9 (2008) 2217–2220.
[40] F. Can, X. Courtois, S. Berland, M. Seneque, S. Royer, D. Duprez, Catal. Today 257 (Part 1) (2015) 41–50.
[41] Y.C. Wei, J. Liu, Z. Zhao, A.J. Duan, G.Y. Jiang, J. Catal. 287 (2012) 13–29.
[42] P. Ning, Z. Song, H. Li, Q. Zhang, X. Liu, J. Zhang, X. Tang, Z. Huang, Appl. Surf. Sci. 332 (2015) 130–137.
[43] F. Liu, H. He, Y. Ding, C. Zhang, Appl. Catal. B: Environ. 93 (2009) 194–204.
[44] K.J. Lee, P.A. Kumar, M.S. Maqbool, K.N. Rao, K.H. Song, H.P. Ha, Appl. Catal. B: Environ. 142 (2013) 705–717.
[45] H. Xu, Q. Zhang, C. Qiu, T. Lin, M. Gong, Y. Chen, Chem. Eng. Sci. 76 (2012) 120–128.
[46] H.S. Roh, W.S. Dong, K.W. Jun, S.E. Park, Chem. Lett. 1 (2001) 88–89.
[47] X. Wu, J. Fan, R. Ran, D. Weng, Chem. Eng. J. 109 (2005) 133–139.
[48] R. Ran, J. Fan, D. Weng, Prog. Nat. Sci. 22 (2012) 7–14.
[49] H. Xu, Y. Wang, Y. Cao, Z. Fang, T. Lin, M. Gong, Y. Chen, Chem. Eng. J. 240 (2014) 62–73.
[50] H. Xu, Z. Qu, C. Zong, W. Huang, F. Quan, N. Yan, Environ. Sci. Technol. 49 (2015) 6823–6830.
[51] S. Li, Q. Hao, R. Zhao, D. Liu, H. Duan, B. Dou, Chem. Eng. J. 285 (2016) 536–543.
[52] Y. Li, H. Cheng, D. Li, Y. Qin, Y. Xie, S. Wang, Chem. Commun. 12 (2008) 1470–1472.
[53] Z. Song, P. Ning, Q. Zhang, H. Li, J. Zhang, Y. Wang, X. Liu, Z. Huang, J. Environ. Sci. 42 (2016) 168–177.
[54] F. Bin, C. Song, G. Lv, J. Song, S. Wu, X. Li, Appl. Catal. B: Environ. 150 (2014) 532–543.
[55] R. Camposeco, S. Castillo, I. Mejía-Centeno, Catal. Commun. 60 (2015) 114–119.
[56] J. Yang, Q. Yang, J. Sun, Q. Liu, D. Zhao, W. Gao, L. Liu, Catal. Commun. 59 (2015) 78–82.
[57] J.P. Dunn, P.R. Koppula, H.G. Stenger, I.E. Wachs, Appl. Catal. B: Environ. 19 (1998) 103–117.
[58] N. Izu, G. Hagen, D. Schoenauer, U. Roeder-Roith, R. Moos, Sensors 11 (2011) 2982–2991.
[59] Q. Wan, L. Duan, K.B. He, J.H. Li, Chem. Eng. J. 170 (2011) 512–517.
[60] Z. Liu, S. Zhang, J. Li, J. Zhu, L. Ma, Appl. Catal. B: Environ. 158–159 (2014) 11–19.
[61] L. Liu, Z. Yao, B. Liu, L. Dong, J. Catal. 275 (2010) 45–60.
[62] W. Lee, G.-N. Bae, Environ. Sci. Technol. 43 (2009) 1522–1527.
[63] M.H. Kim, S.W. Ham, J.B. Lee, Appl. Catal. B: Environ. 99 (2010) 272–278.
[64] N.D. Hutson, B.C. Attwood, K.G. Scheckel, Environ. Sci. Technol. 41 (2007) 1747–1752.
[65] S.J. Yang, Y.F. Guo, N.Q. Yan, Z. Qu, J.K. Xie, C. Yang, J.P. Jia, J. Hazard. Mater. 186 (2011) 508–515.
[66] J.K. Xie, N.Q. Yan, S.J. Yang, Z. Qu, W.M. Chen, W.Q. Zhang, K.H. Li, P. Liu, J.P. Jia, Res. Chem. Intermed. 38 (2012) 2511–2522.
[67] S.J. Yang, N.Q. Yan, Y.F. Guo, D.Q. Wu, H.P. He, Z. Qu, J.F. Li, Q. Zhou, J.P. Jia, Environ. Sci. Technol. 45 (2011) 1540–1546.
[68] J. Wang, Z. Yan, L. Liu, Y. Chen, Z. Zhang, X. Wang, Appl. Surf. Sci. 313 (2014) 660–669.
[69] T. Gu, R. Jin, Y. Liu, H. Liu, X. Weng, Z. Wu, Appl. Catal. B: Environ. 129 (2013) 30–38.
[70] M. Casapu, O. Krocher, M. Mehring, M. Nachtegaal, C. Borca, M. Harfouche, D. Grolimund, J. Phys. Chem. C 114 (2010) 9791–9801.
[71] M. Armandi, B. Bonelli, E. Garrone, M. Ardizzi, F. Cavani, L. Dal Pozzo, L. Maselli, R. Mezzogori, G. Calestani, Appl. Catal. B: Environ. 70 (2007) 585–596.
[72] D. Sun, Q. Liu, Z. Liu, G. Gui, Z. Huang, Appl. Catal. B: Environ. 92 (2009) 462–467.
[73] K. Hadjiivanov, H. Knözinger, Chem. Chem. Phys. 2 (2000) 2803–2806.
[74] W. Shan, F. Liu, H. He, X. Shi, C. Zhang, Appl. Catal. B: Environ. 115 (2012) 100–106.
[75] Z. Liu, H. Su, J. Li, Y. Li, Catal. Commun. 65 (2015) 51–54.
[76] R. Jin, Y. Liu, Z. Wu, H. Wang, T. Gu, Chemosphere 78 (2010) 1160–1166.
[77] X. Zhang, H. He, H. Gao, Y. Yu, Spectrochim. Acta A 71 (2008) 1446–1451.

[78] L. Qu, C. Li, G. Zeng, M. Zhang, M. Fu, J. Ma, F. Zhan, D. Luo, Chem. Eng. J. 242 (2014) 76–85.
[79] W. Chen, Y. Ma, Z. Qu, Q. Liu, W. Huang, X. Hu, N. Yan, Environ. Sci. Technol. 48 (2014) 12199–12205.
[80] H. Fu, X. Wang, H. Wu, Y. Yin, J. Chen, J. Phys. Chem. C 111 (2007) 6077–6085.
[81] H. Chang, X. Chen, J. Li, L. Ma, C. Wang, C. Liu, J.W. Schwank, J. Hao, Environ. Sci. Technol. 47 (2013) 5294–5301.
[82] H. Chang, J. Li, X. Chen, L. Ma, S. Yang, J.W. Schwank, J. Hao, Catal. Commun. 27 (2012) 54–57.
[83] B. Jiang, Z. Wu, Y. Liu, S. Lee, W. Ho, J. Phys. Chem. C 114 (2010) 4961–4965.
[84] E.J. Granite, H.W. Pennline, R.A. Hargis, Ind. Eng. Chem. Res. 39 (2000) 1020–1029.
[85] Z. Liu, Y. Liu, Y. Li, H. Su, L. Ma, Chem. Eng. J. 283 (2016) 1044–1050.